
Implementation of optical quantum gate for polarization-encoded qubits via acousto-optic diffraction by shear acoustic waves in vitreous media

Krupych O., Martynyuk-Lototska I., Orykhivskiy I., Adamenko D., Kostyrko M. and Vlokh R.

O. G. Vlokh Institute of Physical Optics, 23 Dragomanov Street, 79005 Lviv, Ukraine, vlokh@ifp.lviv.ua

Received: 09.09.2021

Abstract. We demonstrate experimentally that acousto-optic diffraction by a shear acoustic wave propagating in fused silica can transform linear or circular polarization states into their orthogonal counterparts. It is also shown that a corresponding acousto-optic cell with a shear acoustic wave propagating in a vitreous medium can be used as a NOT or CNOT gate. The advantage of our method is a possibility for spatial manipulation by qubits via acousto-optic diffraction under condition of changing frequency of the acoustic wave.

Keywords: quantum gates, NOT gates, CNOT gates, acousto-optics, fused silica

UDC: 535.4+534-8+004.04

1. Introduction

Photons are ideal carriers for data bit transfer since they are practically insensitive to interference and can be transmitted over long distances both in open-space and fibre-optic communication lines. In the theory of quantum computing, a term ‘qubit’ or ‘quantum bit’ implies a unit of quantum information, i.e. it is a quantum analogue of bit [1]. A qubit corresponds to a two-level quantum-mechanical system, e.g., to the polarization of single photon which can be linear (vertical or horizontal) and circular (left- or right-handed). In quantum mechanics, quantum state of a qubit can be represented in general by a linear superposition of its two orthonormal basis states (basis vectors). Using a standard Dirac notation, these vectors are typically denoted as ket vectors in the Hilbert space:

$$|0\rangle = \begin{bmatrix} 1 \\ 0 \end{bmatrix}, |1\rangle = \begin{bmatrix} 0 \\ 1 \end{bmatrix}. \quad (1)$$

Unlike a traditional logic state, i.e. a bit which can acquire the values 0 and 1, a qubit can represent any superposition of the two basis states. A linear superposition of these states is a pure state of the qubit. The wave function of the qubit can be written as a ket vector, which is a linear combination of $|0\rangle$ and $|1\rangle$:

$$|\psi\rangle = \alpha|0\rangle + \beta|1\rangle. \quad (2)$$

Here α and β are complex probability amplitudes, the squares of modules of which, $|\alpha|^2$ and $|\beta|^2$, determine the probabilities of quantum system to be in the basis states $|0\rangle$ or $|1\rangle$, respectively. Because the squared amplitudes equate to probabilities, α and β must satisfy the normalization condition

$$|\alpha|^2 + |\beta|^2 = 1. \quad (3)$$

Any two-level quantum system can be used as a qubit. In particular, the qubit can be

implemented physically using a certain state of polarization of a single photon. For example, Jones vectors of a linearly polarized light can be used as basis vectors. If we choose a laboratory Cartesian coordinate system so that its z axis coincides with the horizontal direction of light propagation, the x axis is directed 'horizontally' and the y axis is 'vertical'. Then the electric field vector \mathbf{E} lies in the xy plane, and the polarization of light is described by the projections E_x and E_y on the x and y axes, respectively. The horizontal and vertical linear polarizations of light in this coordinate system are expressed respectively via the Jones vectors \mathbf{J}_H and \mathbf{J}_V :

$$\mathbf{J}_H = \begin{bmatrix} 1 \\ 0 \end{bmatrix}, \quad \mathbf{J}_V = \begin{bmatrix} 0 \\ 1 \end{bmatrix}, \quad (4)$$

while the circular polarizations (left- and right-handed) are given respectively by the Jones vectors \mathbf{J}_L and \mathbf{J}_R [2]:

$$\mathbf{J}_L = \frac{1}{\sqrt{2}} \begin{bmatrix} 1 \\ -j \end{bmatrix}, \quad \mathbf{J}_R = \frac{1}{\sqrt{2}} \begin{bmatrix} 1 \\ j \end{bmatrix}. \quad (5)$$

To implement quantum computing with using of the quantum circuits or quantum computers, one must be able to control the states of qubits. To do this, quantum logic elements (or quantum logic gates) are used. They enable mapping the input states of qubits into the output states according to a certain law. Since the qubit is depicted as a vector in two-dimensional space, the action of the quantum gate can be represented by a unitary matrix, which is multiplied by a corresponding vector of state of the input qubit. Then a single-qubit gate is represented by a 2×2 unitary matrix and a gate which acts on n qubits is given by a $2^n \times 2^n$ matrix.

The simplest single-qubit gates can be described as follows [3]. *Identity gate* is represented by the identity matrix, usually written as \mathbf{I} . It is defined for a single qubit as

$$\mathbf{I} = \begin{bmatrix} 1 & 0 \\ 0 & 1 \end{bmatrix}, \quad (6)$$

where \mathbf{I} is basis-independent and does not modify the quantum state. The identity gate is most useful when describing mathematically the results of various gate operations or when discussing multi-qubit circuits.

The Pauli gates (\mathbf{X} , \mathbf{Y} , \mathbf{Z}) are given by the three Pauli matrices σ_x , σ_y and σ_z . They act on a single qubit. Pauli \mathbf{X} , \mathbf{Y} and \mathbf{Z} equate, respectively, to rotations of the Bloch sphere by π radians around the x , y and z axes. The *Pauli-X* gate is a quantum equivalent of the *NOT gate* in classical computers with respect to the standard basis $|0\rangle$ and $|1\rangle$, which distinguishes the z -axis on the Bloch sphere. It is sometimes called as a bit-flip as it maps $|0\rangle$ to $|1\rangle$ and $|1\rangle$ to $|0\rangle$. This gate is usually represented as

$$\mathbf{X} = \sigma_x = \sigma_1 = \text{NOT} = \begin{bmatrix} 0 & 1 \\ 1 & 0 \end{bmatrix}. \quad (7)$$

Similarly, *Pauli-Y* maps $|0\rangle$ to $i|1\rangle$ and $|1\rangle$ to $-i|0\rangle$. It is given by

$$\mathbf{Y} = \sigma_y = \sigma_2 = \begin{bmatrix} 0 & -i \\ i & 0 \end{bmatrix}. \quad (8)$$

At last, *Pauli-Z* leaves the basis state $|0\rangle$ unchanged and maps $|1\rangle$ to $-|1\rangle$. Due to its nature, it is sometimes called as a phase-flip. This gate is represented as

$$\mathbf{Z} = \sigma_z = \sigma_3 = \begin{bmatrix} 1 & 0 \\ 0 & -1 \end{bmatrix}. \quad (9)$$

Note that the Pauli matrices are involutory, thus meaning that the square of any Pauli matrix is the identity matrix:

$$\mathbf{X}^2 = \mathbf{Y}^2 = \mathbf{Z}^2 = -i\mathbf{XYZ} = \mathbf{I}. \quad (10)$$

Controlled gates act on two or more qubits, where at least one qubit acts as a control for some operation. For example, a *controlled NOT gate* (denoted often as *CNOT* or *CX*) acts on two qubits. It performs *NOT* operation over the second qubit only when the first qubit is $|1\rangle$ and leaves it unchanged otherwise. In the basis

$$|00\rangle = \begin{bmatrix} 1 \\ 0 \\ 0 \\ 0 \end{bmatrix}, |01\rangle = \begin{bmatrix} 0 \\ 1 \\ 0 \\ 0 \end{bmatrix}, |10\rangle = \begin{bmatrix} 0 \\ 0 \\ 1 \\ 0 \end{bmatrix}, |11\rangle = \begin{bmatrix} 0 \\ 0 \\ 0 \\ 1 \end{bmatrix}, \quad (11)$$

the gate is represented by the matrix

$$\text{CNOT} = \begin{bmatrix} 1 & 0 & 0 & 0 \\ 0 & 1 & 0 & 0 \\ 0 & 0 & 0 & 1 \\ 0 & 0 & 1 & 0 \end{bmatrix}. \quad (12)$$

The value of the second (controlled) qubit after the action of *CNOT* coincides with the result of action of a classical logical operation XOR (exclusive disjunction). The *CNOT* gate can be described as a gate that maps the basis states $|a,b\rangle \mapsto |a, a \otimes b\rangle$, where \otimes is XOR. Unlike the classic logic gate, which has a unit output, *CNOT* has two outputs, which preserves reversibility of the computations. *CNOT* can be used to untangle the Bell states (i.e., to remove quantum entanglement). In general, any quantum circuit included in a quantum computer can be simulated with a combination of only *CNOT* elements and rotations of individual qubits. In some important cases, quantum computing allows one to speed up significantly the calculations and so solve many problems that cannot be solved by means of classical computers. Therefore, development of the physical systems that enable implementation of the basic elements of quantum computing is an important task.

The *CNOT* gate can be based on different physical principles. For instance, the qubits can be constructed using nuclear spins in an NMR processor [4, 5], cold trapped ions and atoms [6–8], biomolecular systems [9], superconducting circuits [10, 11], etc. All of these principles reveal both advantages and shortcomings. In particular, the cold trapped atoms and ions, similarly to the superconducting circuits, need low-temperature keeping of their working elements, while the biomolecular systems are not stable with respect to temperature changes. From this point of view, photons which are insensitive to external influences seem to be one of the best carriers for quantum computing. Moreover, photons possess both spin and orbital angular momentums, which can form entangled intra-system and inter-system states [12, 13].

A *CNOT* gate utilizing photons as carriers has been offered in Ref. [14]. In this work, a half-wave plate and a polarization beam splitter have been used in order to implement this gate. In Ref. [15], a new design of quantum optical gate for manipulating by two-qubit entanglement has been suggested. A first experimental realization of the *CNOT* gate with no interferometry has been demonstrated in the work [16]. These works deal with bulk optical elements such as half-wave plates or polarization beam splitters, which need precise alignment. These disadvantages can be eliminated when using an integrated optic technology [17–20]. An integrated optical quantum-logic element has been suggested in the study [21]. Unfortunately, this scheme needs optically birefringent waveguides and keeping the coefficients of branching with high accuracy, which

requires complex high-technological equipment when fabricating the integrated optical quantum gates. Moreover, all of the optical schemes mentioned above do not allow operating the direction of light propagation, although the latter would make possible spatial manipulation of qubits, e.g. their multiplexing or addressing.

From this viewpoint, acousto-optic (AO) Bragg diffraction is probably the best method for light-beam scanning. Here one can change the angle of diffraction when changing the frequency of an acoustic wave (AW). In the present work, we describe a new technique for implementing an optical quantum gate and controlling polarization-encoded qubits, which is based on the AO interactions. The method [22] can be implemented using either volume optical or integrated optical devices.

2. Fundamentals of the method

Let the electric field vector of the incident light wave lie in the xy plane and its polarization be defined by the complex 2×1 Jones vector \mathbf{J}_{in} :

$$\mathbf{J}_{\text{in}} = \begin{bmatrix} \tilde{E}_x^{\text{in}} \\ \tilde{E}_y^{\text{in}} \end{bmatrix}, \quad (13)$$

where \tilde{E}_x^{in} and \tilde{E}_y^{in} are the complex Cartesian amplitudes of the electric field.

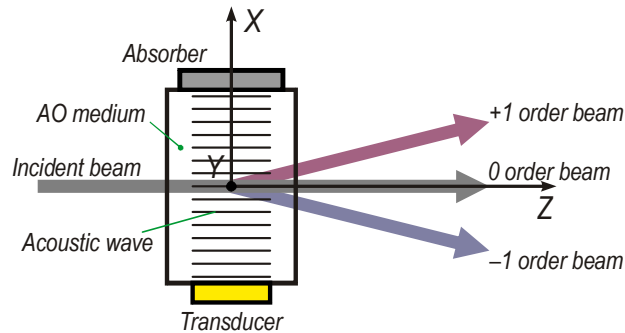


Fig. 1. Schematic view of AO Bragg diffraction in a vitreous medium and a laboratory coordinate system xyz .

Imagine that a transverse AW propagates almost perpendicular to the z axis and close to the x axis. Let its polarization be vertical, i.e. the displacement vector is oriented along the y axis. When this AW propagates in a solid material medium, the refractive index of the material is modulated due to elasto-optic effect. The change in the refractive index is determined by the amplitude of AW and the components of elasto-optic tensor \mathbf{P} . In case of isotropic materials like glass (or cubic crystals described by the point symmetry groups 432 , $\bar{4}3m$ and $m3m$), the mentioned tensor has the form

$$\mathbf{P} = \begin{bmatrix} p_{11} & p_{12} & p_{12} & 0 & 0 & 0 \\ p_{12} & p_{11} & p_{12} & 0 & 0 & 0 \\ p_{12} & p_{12} & p_{11} & 0 & 0 & 0 \\ 0 & 0 & 0 & p_{44} & 0 & 0 \\ 0 & 0 & 0 & 0 & p_{44} & 0 \\ 0 & 0 & 0 & 0 & 0 & p_{44} \end{bmatrix}. \quad (14)$$

In the case of anisotropic AO Bragg diffraction by a transverse (i.e., shear) AW, the polarization of the diffracted optical wave differs from that of the light beam incident on the AO cell [23]. In the case of isotropic diffraction in vitreous medium, the change in the light polarization can take place, too. Let us choose the laboratory Cartesian coordinate system xyz so that the input light beam propagates along the z axis (see Fig. 1). The relation for the electric field of the diffracted optical wave can be written as

$$E_1^d = \Delta B_{12} D_2^{in} = p_{66} e_6 D_2^{in}, p_{66} = p_{44}. \quad (15)$$

where D_2^{in} is the electrical induction of the incident optical wave, p_{44} the effective elasto-optic coefficient, and e_6 the strain-tensor component caused by the transverse AW propagating along the x axis. For the incident optical wave polarized parallel to the x axis we have $E_2^d = \Delta B_{21} D_1^{in} = p_{44} e_6 D_1^{in}$. As seen from Eq. (15), the polarization of the diffracted wave is orthogonal to the polarization of the incident wave even in the isotropic medium.

In the above geometry of AO interaction in a glass medium, the diffraction efficiency is defined by the effective elasto-optic constant p_{44} , whereas the polarization of the diffracted wave in general differs from that of the input optical wave. When the polarization of the incident wave is linear and is oriented along the vertical direction, the diffracted wave has the horizontal polarization, and vice versa:

$$\mathbf{J}_H^{in} \rightarrow \mathbf{J}_V^d, \mathbf{J}_V^{in} \rightarrow \mathbf{J}_H^d. \quad (16)$$

When the input light has the left circular polarization, then the diffracted light reveals the right circular polarization, and vice versa:

$$\mathbf{J}_L^{in} \rightarrow \mathbf{J}_R^d, \mathbf{J}_R^{in} \rightarrow \mathbf{J}_L^d. \quad (17)$$

These polarization transformations occurring under AO diffraction can be described by the unitary transformation matrix, i.e. the Jones matrix \mathbf{T} of the type

$$\mathbf{T} = \begin{bmatrix} 0 & 1 \\ 1 & 0 \end{bmatrix}. \quad (18)$$

Note that this matrix is equivalent to the Jones matrix of a half-wave plate oriented in a so-called ‘diagonal’ position (i.e., at the angle $\pi/4$ with respect to the x axis). Such a half-wave plate converts any incoming polarization ellipse, with the azimuth φ of its major axis and the ellipticity e , into the output ellipse described by the azimuth $(\pi/2 - \varphi)$ and the ellipticity $(-e)$. This means that only the polarizations located at a ‘big circle’ HRVL (Horizontal linear – Right circular – Vertical linear – Left circular) of the Poincare sphere, i.e. the polarizations having the orientations of their major axes along either x or y axes (in other terms, having the azimuths $\varphi = 0$ or $\varphi = \pi/2$) are mapped onto their orthogonal polarization states. For example, the polarization ellipse with the horizontal major axis ($\varphi = 0$) and the ellipticity e is converted into the ‘vertical’ ellipse ($\varphi = \pi/2$) with the opposite ellipticity $(-e)$. As a result, the pairs of the orthogonal states of photon polarization referred to as ‘horizontal–vertical linear polarizations’ or ‘left–right circular polarizations’ can be chosen as the basis states of the qubit.

To verify a practical performance of such an AO cell, we have conducted the experiments described below.

3. Experimental procedures and the main results

We have studied the behaviour of light polarization in the course of AO diffraction of polarized light in fused silica. A shear AW propagates along the horizontal direction that coincides with the x axis of our laboratory coordinate system. The displacement vector (i.e., the polarization) of the AW is oriented vertically, i.e. along the y axis. A lithium niobate transducer with the dimensions $5 \times 3 \text{ mm}^2$ and the resonant frequency 50 MHz is used to excite a transverse ultrasonic AW. The incident light beam of a He-Ne laser with the wavelength 633 nm is directed normally to the AW in the horizontal plane, i.e. along the z axis.

The polarization of probing light has been prepared by means of a linear polarizer followed

by a quarter-wave plate. Such a polarization generator is able to implement any polarized state. The polarization states of the diffracted beams with the orders 0 and -1 have been analyzed by means of a rotating-analyzer technique. To determine the parameters of the output polarization ellipse (i.e., the ellipticity angle ε and the azimuthal angle θ of the major axis, which is counted counter-clockwise beginning from the x axis), we have used experimental dependences of the light intensity I recorded with photodetector on the analyzer azimuth a . These dependences can be fitted with a standard function

$$I = I_0 \{1 + \cos 2\varepsilon \cos [2(a - \theta)]\} / 2, \quad (19)$$

where I_0 denotes the intensity of the light incident on the analyzer. In this manner, the orientation and the ellipticity of the polarization ellipse have been determined.

Three kinds of probing light beams have been used in our experiments. First, we utilize a linearly polarized light. In this configuration, the quarter-wave plate is removed from the polarization generator. Six azimuthal positions of the input polarizer have been used: 0° , 45° , 90° , 135° , 30° and 60° . The parameters of the polarization ellipse of the light outgoing from the sample (namely, the azimuth θ , the ellipticity angle ε and the ellipticity $e = \tan(\varepsilon)$) have been determined under the following experimental conditions: (a) no ultrasound signal is applied (i.e., no AO diffraction occurs), (b) a zero-order beam under ultrasound signal applied, and (c) a diffracted beam of the order -1 under ultrasound signal applied. The results obtained for the case of linearly polarized incident light are collected in Table 1 and Fig. 2.

Table 1. Polarization parameters of AO-diffracted optical beams, as measured for the case of linearly polarized input light.

№	Azimuth p of input polarization, deg	Azimuth θ , deg	Output polarization		
			Ellipticity angle ε , deg	Ellipticity e	
1	$p = 0$	no diffraction	0.47 ± 0.16	6.2×10^{-4}	1.1×10^{-5}
		0 order	0.68 ± 0.05	1.55	0.027
		-1 order	90.38 ± 0.10	5.57	0.097
2	$p = 90$	no diffraction	90.44 ± 0.05	1.6×10^{-4}	2.7×10^{-6}
		0 order	90.35 ± 0.03	3.8×10^{-5}	6.6×10^{-7}
		-1 order	0.50 ± 0.13	4.45	6.6×10^{-7}
3	$p = 45$	no diffraction	45.49 ± 0.04	0.83	0.015
		0 order	45.45 ± 0.03	1.2×10^{-4}	2.1×10^{-6}
		-1 order	44.74 ± 0.06	2.09	0.037
4	$p = 135$	no diffraction	135.46 ± 0.04	1.17	0.020
		0 order	135.48 ± 0.05	1.01	0.018
		-1 order	134.61 ± 0.13	3.55	0.062
3	$p = 30$	no diffraction	31.15 ± 0.38	2.2×10^{-4}	3.9×10^{-6}
		0 order	30.24 ± 0.15	1.2×10^{-4}	2.1×10^{-6}
		-1 order	60.09 ± 0.20	3.60	0.063
4	$p = 60$	no diffraction	60.78 ± 0.27	0.33	5.8×10^{-3}
		0 order	60.61 ± 0.19	0.21	3.7×10^{-4}
		-1 order	30.57 ± 0.35	2.78	0.049

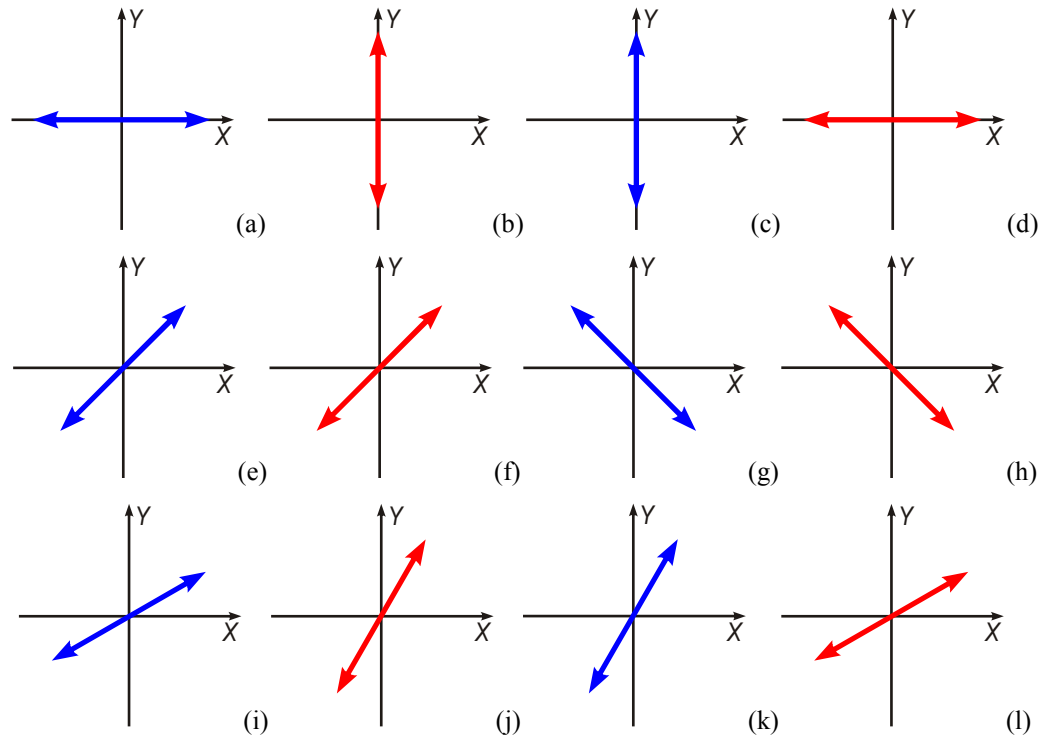


Fig. 2. Changes in the polarization of linearly polarized light occurring in the course of AO diffraction: panels (a), (c), (e), (g), (i) and (k) correspond to incident light polarization, and panels (b), (d), (f), (h), (j) and (l) to diffracted light polarization.

After that, a circularly polarized probing light has been used. To provide a circular polarization, the quarter-wave plate has been inserted after the polarizer and in front of the material sample. The fast axis of the quarter-wave plate has been oriented in the azimuthal position $c = 0^\circ$. The circularly polarized probing beams with the two alternative (left or right) handednesses have been prepared via setting the polarizer into the azimuthal positions $p = 45^\circ$ or $p = 135^\circ$, respectively. The parameters θ , ε and e of the polarization ellipse have been determined under the same experimental conditions. The results obtained for the case of circularly polarized incident light are gathered in Table 2 and Fig. 3.

Table 2. Polarization parameters of AO-diffracted optical beams, as measured for the case of circularly polarized input light.

№	Input polarization	Output polarization		
		Azimuth θ , deg	Ellipticity angle ε , deg	Ellipticity e
1	Left-handed circular			
	no diffraction	2.927±0.558	43.753	0.9574
	0 order	1.216±1.912	43.574	0.9514
	-1 order	46.507±3.852	-44.143	-0.9705
2	Right-handed circular			
	no diffraction	1.683±1.436	-44.146	-0.9706
	0 order	2.174±1.878	-43.872	-0.9614
	-1 order	38.331±3.177	44.527	0.9836

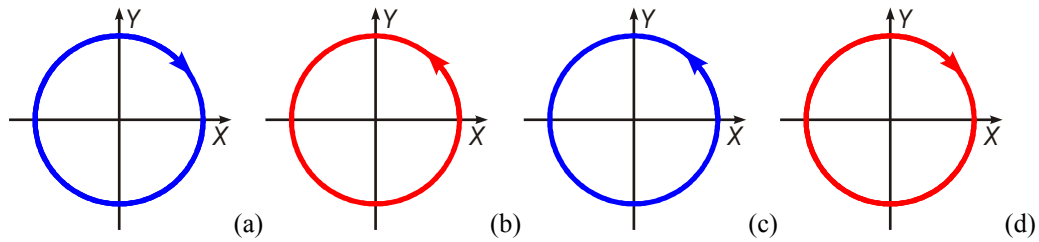


Fig. 3. Changes in the polarization of circularly polarized light occurring in the course of AO diffraction: panels (a) and (c) correspond to incident light polarization, and panels (b) and (d) to diffracted light polarization.

Finally, the elliptically polarized probing light has been used. Then the fast axis of the quarter-wave plate remains in the azimuthal position $c = 0^\circ$. The elliptically polarized probing light with the two azimuths, 0° and 90° , has been prepared via setting the polarizer into the azimuthal positions $p = 25^\circ$ and $p = 65^\circ$, respectively. Then the parameters θ , ε and e under interest have been determined. The results obtained for the case of elliptically polarized incident light are reported in Table 3 and Fig. 4.

Table 3. Polarization parameters of AO-diffracted optical beams, as measured for the case of elliptically polarized input light.

№	Input polarization	Output polarization		
		Azimuth θ , deg	Ellipticity angle ε , deg	Ellipticity e
1	$p = 25^\circ, c = 0^\circ (\theta = 0^\circ, e = 0.466)$			
	no diffraction	0.46 ± 0.11	25.16 ± 0.09	0.470
	0 order	0.87 ± 0.32	25.51 ± 0.27	0.477
	-1 order	91.93 ± 0.14	-25.34 ± 0.11	-0.474
2	$p = 65^\circ, c = 0^\circ (\theta = 90^\circ, e = -0.466)$			
	no diffraction	90.55 ± 0.16	-24.51 ± 0.12	-0.456
	0 order	90.79 ± 0.29	-24.62 ± 0.29	-0.458
	-1 order	1.88 ± 0.17	25.16 ± 0.17	0.470

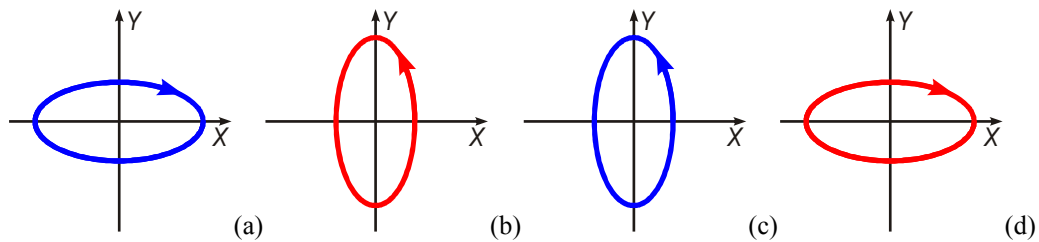


Fig. 4. Changes in the polarization of elliptically polarized light occurring in the course of AO diffraction: panels (a) and (c) correspond to incident light polarization, and panels (b) and (d) to diffracted light polarization.

4. Discussion

Having analyzed the data presented in Table 1, one can conclude that, in case of the AO diffraction in fused silica, the linearly polarized incident light with the horizontal polarization ($\theta = 0^\circ$) is mapped into the vertical polarization ($\theta = 90^\circ$), and vice versa. The ‘diagonal’ linear polarizations given by $\theta = 45^\circ$ or $\theta = 135^\circ$ do not change their polarizations under the AO interaction. The

analysis of the transformations of circularly polarized incident light at the AO diffraction gathered in Table 2 draws the conclusion that the polarizations of the diffracted beams remain circular, but their handednesses are inverted, i.e. the sign of the ellipticity e changes from +1 to -1, and vice versa. Finally, as seen from Table 3, the AO diffraction converts the polarization ellipses with the horizontal (the azimuth $\theta = 0^\circ$) or vertical ($\theta = 90^\circ$) directions of their major axes into the ellipses with the opposite signs of ellipticity and the orthogonal major axes.

In other words, the experimental results obtained in this work confirm that the AO cell with the shear AWs in vitreous media acts on the light polarization like a half-wave plate in a diagonal position, i.e. it is described by the Jones matrix (18). It is obvious that the Jones matrix \mathbf{T} given by Eq. (18) is identical to the matrix of the quantum *NOT* gate (the *Pauli-X* gate – see Eq. (7)). Therefore, the AO cell with the shear AW propagating in a vitreous medium can be used as a quantum *NOT* gate for the polarization-encoded qubits. Finally, in the absence of ultrasonic AW, the light polarization does not change, whereas application of the acoustic signal converts the light polarization into its orthogonal counterpart, so that we obtain a controlled *NOT* gate denoted as a *CNOT* gate.

5. Conclusion

In the present work, we have shown experimentally that the AO diffraction by the shear AW propagating in fused silica changes the linear and circular polarization states to the orthogonal polarizations. In the course of Bragg diffraction, the elliptical polarization states with the ‘horizontal’ and ‘vertical’ azimuths are converted into the elliptical polarization states with the opposite signs of ellipticity and the orthogonal directions of their major axes. As a result, the AO cell with the shear AW propagating in a vitreous medium can be used as the quantum *NOT* gate for the polarization-encoded qubits. Moreover, one can easily obtain the *CNOT* gate since the light polarization does not change in the absence of ultrasonic wave and the polarization is converted into its orthogonal counterpart whenever the acoustic signal is applied. The advantage of our method consists in a ready possibility for spatial manipulation by the qubits via the AO diffraction occurring with changing frequency of the AW.

Acknowledgement

The authors acknowledge financial support of this study from the Ministry of Education and Science of Ukraine under the Projects # 0121U109804 and #0120U102031.

References

1. Schumacher B, 1995. Quantum coding. *Phys. Rev. A*. **51**: 2738–2747.
2. Azzam R M A and Bashara N M. *Ellipsometry and Polarized Light*. Amsterdam, New York, Oxford: North Holland Publ. Company, 1977.
3. Barenco A, Bennett C H, Cleve R, DiVincenzo D P, Margolus N, Shor P, Sleator T, Smolin J A and Weinfurter H, 1995. Elementary gates for quantum computation. *Phys. Rev. A*. **52**: 3457–3467.
4. Chuang I L, Sherwood M H, Yannoni C S, Nuclear magnetic resonance quantum computing method with improved solvents. United States Patent No. US 6,218,832 B1, Apr. 17, 2001.
5. Guanru Feng, Guofu Xu and Guilu Long, 2013. Experimental realization of nonadiabatic holonomic quantum computation. *Phys. Rev. Lett.* **110**: 190501.
6. Cirac J I and Zoller P, 1995. Quantum computation with cold trapped ions. *Phys. Rev. Lett.* **74**: 4091–4094.

7. Monroe C, Meekhof D M, King B E, Itano W M, and Wineland D J, 1995. Demonstration of a fundamental quantum logic gate. *Phys. Rev. Lett.* **75**: 4714–4717.
8. Schmidt-Kaler F, Haffner H, Riebe M, Gulde S, Lancaster G P T, Deuschle T, Becher C, Roos C F, Eschner J and Blatt R, 2003. Realization of the Cirac–Zoller controlled-NOT quantum gate. *Nature*. **422**: 408–411.
9. Moseley F, Halamek J, Kramer F, Poghossian A, Schoninger M J and Katz E, 2014. An enzyme-based reversible CNOT logic gate realized in a flow system. *Analyst*. **139**: 1839–1842.
10. Bækkegaard T, Kristensen L B, Loft N J S, Andersen C K, Petrosyan D and Zinner N T, 2019. Realization of efficient quantum gates with a superconducting qubit-qutrit circuit. *Sci. Rep.* **9**: 13389.
11. Wendin G, 2017. Quantum information processing with superconducting circuits: a review. *Rep. Prog. Phys.* **80**: 106001.
12. D’Ambrosio V, Carvacho G, Graffitti F, Vitelli C, Piccirillo B, Marrucci L and Sciarrino F, 2016. Entangled vector vortex beams. *Phys. Rev. A*. **94**: 030304(R).
13. Skab I, Kostyrko M and Vlokh R, 2020. Single-photon entanglement at acousto-optic (acousto-gration) diffraction. *Ukr. J. Phys. Opt.* **21**: 152–158.
14. Biswas K K and Shihaan S, 2012. Design and realization of a quantum controlled NOT gate using optical implementation. *Int. J. Adv. Res. & Technol.* **1**: 1–9.
15. Langford N K, Weinhold T J, Prevedel R, Resch K J, Gilchrist A, O’Brien J L, Pryde G J and White A G, 2005. Demonstration of a simple entangling optical gate and its use in Bell-state analysis. *Phys. Rev. Lett.* **95**: 210504.
16. Okamoto R, Hofmann H F, Takeuchi S and Sasaki K, 2005. Demonstration of an optical quantum controlled-NOT gate without path interference. *Phys. Rev. Lett.* **95**: 210506.
17. Politi A, Martin J C, Rarity J G, Siyuan Yu and O’Brien J L, 2008. Silica-on-silicon waveguide quantum circuits. *Science*. **320**: 646–649.
18. Politi A, Matthews J C and O’Brien J L, 2009. Shor’s quantum factoring algorithm on a photonic chip. *Science*. **325**: 1221–1221.
19. Matthews J C, Politi A, Stefanov A and O’Brien J L, 2009. Manipulation of multiphoton entanglement in waveguide quantum circuits. *Nature Photon.* **3**: 346–350.
20. Sansoni L, Sciarrino F, Vallone G, Mataloni P, Crespi A, Ramponi R and Osellame R, 2010. Polarization entangled state measurement on a chip. *Phys. Rev. Lett.* **105**: 200503.
21. Crespi A, Mataloni P, Ramponi R, Sansoni L, Sciarrino F, Vallone G and Osellame R. Integrated optics logic gate for polarization-encoded quantum qubits and a method for the production and use thereof. U.S. Patent Application No. 14/115, 622, 2014.
22. Krupych O M, Martynyuk-Lototska I Y, Kostyrko M E, Vasylyuk Yu V and Vlokh R O. Method of implementing optical quantum logic element for control of qubits with polarization coding. Application for the Invention of Ukraine, 2021, a202103404.
23. Magdich L N and Molchanov V Ya. *Acoustooptic Devices and Their Applications*. New York, London, Paris, Montreux, Tokyo, Melbourne: Gordon and Breach Science Publ., 1989.

Krupych O., Martynyuk-Lototska I., Orykhivskiy I., Adamenko D., Kostyrko M. and Vlokh R. 2021. Implementation of optical quantum gate for polarization-encoded qubits via acousto-optic diffraction by shear acoustic waves in vitreous media. *Ukr.J.Phys.Opt.* **22**: 198 – 208. doi: 10.3116/16091833/22/4/198/2021

Анотація. Експериментально продемонстровано, що акустооптична дифракція на зсувній акустичній хвилі, яка поширюється в плавленому кварці, може перетворити лінійні або кругові поляризаційні стани на їхні ортогональні аналоги. Також показано, що відповідну акустооптичну комірку з зсувною акустичною хвилею, яка поширюється у склоподібному середовищі, можна використовувати як квантові вентиля NOT або CNOT. Перевагою нашого методу є можливість просторового керування кубітами за допомогою акустооптичної дифракції за умови зміни частоти акустичної хвилі.